



Efficient solar photocatalytic degradation of textile wastewater using ZnO/ZTO composites



Supamas Danwittayakul^a, Mayuree Jaisai^b, Joydeep Dutta^{b,c,*}

^a National Metal and Materials Technology Center, 114 Thailand Science Park, Klong Nueng, Klong Luang, Pathumthani 12120, Thailand

^b Center of Excellence in Nanotechnology, Asian Institute of Technology, P.O. Box 4, Klong Luang, Pathumthani 12120, Thailand

^c Chair in Nanotechnology, Water Research Center, Sultan Qaboos University, P.O. Box 17, 123 Al-Khoudh, Sultanate of Oman, Oman

ARTICLE INFO

Article history:

Received 28 January 2014

Received in revised form 9 July 2014

Accepted 21 July 2014

Available online 27 July 2014

Keywords:

Zinc oxide

Zinc tin oxide

Photocatalysis

Photocatalytic activity

Degradation efficiency

ABSTRACT

Zinc oxide/zinc tin oxide (ZnO/ZTO) nanocomposites were synthesized on porous ceramic support using a simple and economical hydrothermal technique for photocatalytic degradation of organic dyes. One dimensional ZnO nanorods were grown epitaxially on ZnO nanoparticles seeded substrates in a chemical bath with different growth solution concentrations followed by the synthesis of zinc tin oxide (ZTO) in an autoclave. Comparison of photocatalytic activity of pure ZnO nanorod catalysts with different dimensions on the degradation of methylene blue showed that ZnO nanorods (ZnO20 mM) with the highest specific surface area ($45 \text{ m}^2 \text{ g}^{-1}$) are 13% more active than those with lower surface areas ZnO nanorod catalysts (ZnO1 mM, ZnO5 mM and ZnO10 mM; $20\text{--}39 \text{ m}^2 \text{ g}^{-1}$). To further enhance photocatalytic activity, we composited ZnO with ZTO and found that ZnO/15ZTO can be a better photocatalyst improving 16% degradation efficiency attributed to the reduction of electron–hole recombination by charge carrier separation in the composites. Moreover, ZnO/15ZTO showed 50% Photocatalytic degradation efficiency and 77% COD removal of textile waste water when irradiated by sunlight. ZnO/ZTO monolith shows much promise to be an attractive photocatalyst for solar photocatalytic application.

© 2014 Elsevier B.V. All rights reserved.

1. Introduction

Textile industries traditionally use a huge amount of water and approximately two percent of dyes that are discharged directly in industrial effluent of which, about 10% are lost during the dyeing process [1]. The dyes are therefore released into the environment that can lead to adverse effects on the ecosystem due to the toxicity [2]. In addition, the wastewater generated from the textile industry is generally high in both biochemical oxygen demand (BOD) and chemical oxygen demand (COD) because it comprises spent textile dyes, suspended solids, mineral oils, electrolytes, surfactants, etc. [3,4].

Photocatalysis has attracted a lot of attention as effective process in the mitigation of environmental pollution. Photocatalysis is a light induced catalytic process that reduces or oxidize organic molecules through redox reactions activated through the electron–hole pairs generated on the surface of metal oxide

semiconductors upon beyond band gap light irradiation [5]. Zinc oxide (ZnO) is a promising candidate as a solar light photocatalytic material since it demonstrates high photocatalytic efficiencies for the degradation of organic pollutants [6–9] in comparison to other metal oxides [10,11]. Surface area and surface defects of metal oxides are important factors for enhanced photocatalytic activity [9,12,13]. The higher effective surface area leads to higher adsorption of organic molecules, while enhanced photocatalytic activities lead to its efficient degradation. Though ZnO has been synthesized by several techniques, hydrothermal synthesis is preferred for many applications since it is a low temperature, green and simple process to obtain controlled nanostructures [14]. Diverse nanostructures of ZnO such as nanorods, nanowires and nanoflowers have been synthesized by controlling reaction conditions in a hydrothermal process [14]. One-dimensional ZnO nanorods as compared to nanoparticles on supported substrates are reported to enhance photocatalytic activity due to larger effective surface area [15,16].

Different techniques have been used to achieve visible light absorption in these high bandgap materials such as metal and non-metal doping, semiconductor coupling, surface sensitization, increasing crystal defects and precious metal deposition to increase the photodegradation activity under visible light. Direct

* Corresponding author at: Chair in Nanotechnology, Water Research Center, Sultan Qaboos University, P.O. Box 17, 123 Al-Khoudh, Sultanate of Oman.

Tel.: +66 2 524 5680/+968 24143266; fax: +66 2 524 5617/+968 24413532.

E-mail addresses: dutta@squ.edu.om, nanosqu@gmail.com (J. Dutta).

photoexcited electron–hole flow by coupling metal oxides to match the electrochemical potential of coupled semiconductors is a promising method to improve photocatalytic activities. Zinc stannate (ZnSn_2O_4), called zinc tin oxide (ZTO), a ternary oxide semiconductor with wide bandgap (~ 3.6 eV), has been utilized in wide applications included photocatalysis for the degradation of organic pollutants [17,18] due to its chemical stability and high electron mobility [19] that are essential for enhanced photocatalysis. Synthesis of ZTO nanostructures have been studied through different techniques such as sol–gel [20], thermal evaporation [21] and hydrothermal methods [12,22–25]. ZnO and ZTO (ZnO/ZTO) composite oxides have been used as photocatalysts with better activity for the degradation of organic contaminants in water that was attributed to the formation of hetero-junctions between ZnO and ZTO leading to an increase in photocatalytic activity [23,26,27]. Moreover, the synergistic effect of multi-metal oxides play an important role to hinder the electron–hole recombination [28,29]. Although a lot of research targeted to the development of novel photocatalysts to improve the efficiency, there are still very few reports focused on real world photocatalytic applications for the depollution of textile wastewater.

In this work, ZnO, and ZnO/ZTO composite oxide were synthesized on porous ceramic monoliths through hydrothermal method with different concentrations of precursor solutions. Photocatalytic activity of each prepared catalyst was determined by monitoring the reduction of absorption peak at specific wavelength of aqueous methylene blue solutions. Characteristic of all catalysts were examined and reported in this study. In addition, textile wastewater was collected from industrial company and treated using ZnO/ZTO composite under the sunlight and the results are also discussed in this work.

2. Experimental

2.1. Materials

All the chemicals used for synthesis of the catalysts were of analytical grade and used as-received without any further purification. Chemicals used in this work are zinc acetate dihydrate ($\text{Zn}(\text{CH}_3\text{COO})_2 \cdot 2\text{H}_2\text{O}$), ethanol ($\text{C}_2\text{H}_5\text{OH}$) and zinc nitrate hexahydrate ($\text{Zn}(\text{NO}_3)_2 \cdot 6\text{H}_2\text{O}$) from Merck, tetrachloride pentahydrate ($\text{SnCl}_4 \cdot 5\text{H}_2\text{O}$), sodium hydroxide (NaOH) from Univar and hexamethylene tetramine ($\text{C}_6\text{H}_{12}\text{N}_4$) from Sigma-Aldrich. Cordierite ceramic (magnesium iron aluminium cyclosilicate) with honeycomb structure was procured from Zhongtian Co., Ltd. was used as a substrate throughout this study.

2.2. Hydrothermal synthesis of ZnO nanorods

ZnO nanorods were synthesized on porous cordierite ceramic substrates by a hydrothermal process described in our previous work [14,30]. Spherical ZnO nanoparticles were first deposited as a seed layer by thermal decomposition of zinc acetate. The ceramic substrates were dipped in 2 mM zinc acetate solution in ethanol for 10 min and then heated at 400°C for 10 min. This cycle was repeated several times until a uniform seed layer was deposited. ZnO nanorods were then grown epitaxially from the seed layer by hydrothermal process using equimolar (1–20 mM) solution of zinc nitrate hexahydrate ($\text{Zn}(\text{NO}_3)_2 \cdot 6\text{H}_2\text{O}$) and hexamethylene tetramine ($\text{C}_6\text{H}_{12}\text{N}_4$) as a source of precursors [14,31]. The pH of growth solutions were controlled at the level of 6.2–6.6 prior to the growth stage by adjusting the solution with dilute nitric acid (HNO_3) [32]. Hydrothermal growth was then conducted at a temperature of 95°C for 15 h in a sealed chemical bath. Equimolar (1–20 mM) solution of zinc nitrate and hexamine was replenished

Table 1

Assigned sample numbers and details of the sample preparation conditions.

Sample code	Synthesis condition		
	Precursors	Temp.	Time
ZnO1 mM	1 mM Zn^{2+}	95°C	15 h
ZnO5 mM	5 mM Zn^{2+}	95°C	15 h
ZnO10 mM	10 mM Zn^{2+}	95°C	15 h
ZnO20 mM	20 mM Zn^{2+}	95°C	15 h
ZnO/5ZTO	5 mM Sn^{4+}	120°C	4 h
ZnO/10ZTO	10 mM Sn^{4+}	120°C	4 h
ZnO/15ZTO	15 mM Sn^{4+}	120°C	4 h

every 5 h to ascertain the ready availability of zinc ions in the growth solution. ZnO nanorods grown on the substrates were annealed at 350°C for 1 h in an atmospheric oven. The details of samples and its assigned numbers are summarized as in Table 1.

2.3. Hydrothermal synthesis of ZnO/ZTO nanocomposite

For the ZTO growth, the ZnO nanorod coated substrates were typically synthesized in 5 mM growth solution for 15 h (ZnO5 mM). Hydrothermal synthesis of zinc tin oxide (ZTO) on ZnO nanorods (ZnO/ZTO) was carried out in an autoclave as shown in Fig. 1. Aqueous solutions of tin tetrachloride pentahydrate and sodium hydroxide solutions were prepared in deionized water. Molar ratio of NaOH to SnCl_4 was controlled at 10:1. Zinc tin oxide (ZTO) was synthesized on ZnO nanorods with three different Sn^{4+} concentrations (5 mM, 10 mM and 15 mM) in the autoclave. pH of the solutions were controlled at about 10 by titrating with sodium hydroxide solution. ZnO nanorods on porous substrates (ZnO5 mM) were immersed in the autoclave heated to 120°C for 4 h followed by annealing at 350°C for 1 h in air. The details of samples and its assigned numbers are summarized as in Table 1.

2.4. Characterization

Each specimen was investigated using field emission scanning electron microscope (FESEM, JEOL-6301) working at 20 KV to record the morphology of nanorods. Shape and sizes of ZnO nanorods were determined by considering a sample of 60 nanorods from 3 micrographs using standard image analysis software (I-solution software). The specimens were also investigated using transmission electron microscope (TEM, JEOL JEM-2010) working at 200 KV to confirm the crystal structure of the nanocatalysts. X-ray diffraction (XRD) of as-prepared ZnO nanorod samples were performed on a PAnalytical X'Pert PRO X-ray diffractometer with $\text{Cu K}\alpha$ radiation with 0.5 second of count time and 0.02 degree of step angle. Specific surface areas (SSA) of substrates were determined

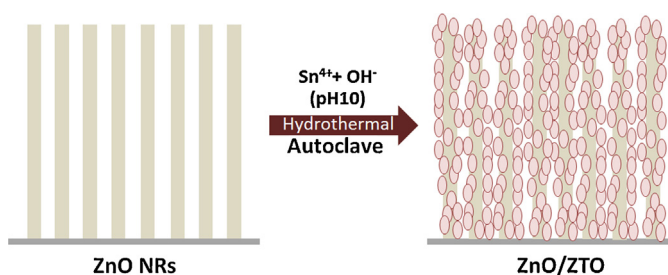


Fig. 1. Schematic representation of ZnO/ZTO nanocomposite synthesis by hydrothermal technique. First ZnO nanorods were grown in an equimolar solution of zinc nitrate and hexamine at 95°C for 15 h (fresh precursors were added every 5 h). Then the ZTO coating was done with aqueous solutions of tin tetrachloride pentahydrate and sodium hydroxide solution with the nanorods being the zinc source at 120°C for 4 h.

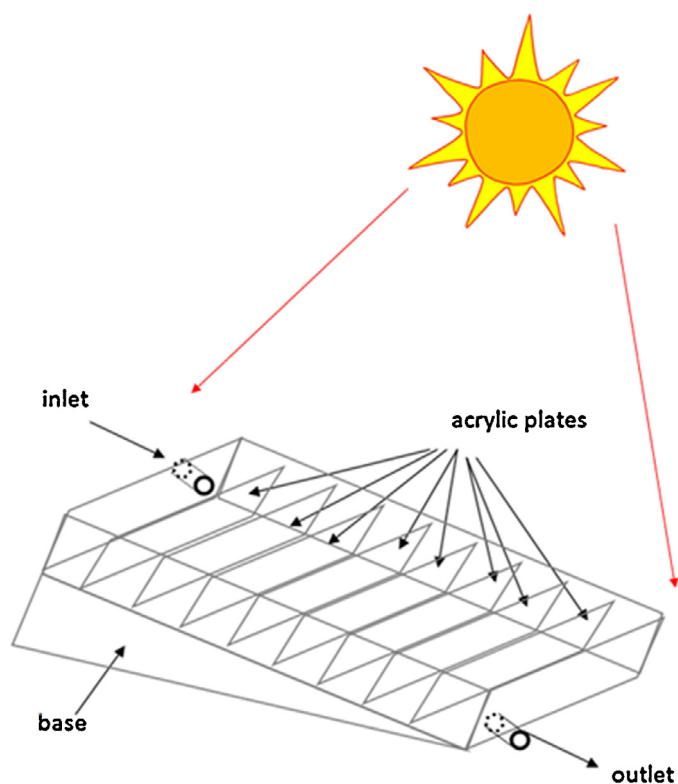


Fig. 2. Schematic view of the wastewater treatment bath, rectangular in shape (length 30 cm, width 20 cm and height 5 cm). The base of treatment bath is 15 degree inclined to the floor. The acrylic plates are placed to increase the residence time of the wastewater in the bath.

using N_2 gas adsorption technique (Autosorb-1C; Quantachrome Ins.).

2.5. Photocatalysis tests

2.5.1. Artificial wastewater

Photocatalytic activity was evaluated under visible light irradiation with a popular test dye, methylene blue ($C_{16}H_{18}N_3SCl$). A $10 \mu M$ solution of methylene blue was prepared in deionized water and put in a test cuvette and each photocatalyst sample ($0.5 \text{ cm} \times 4.0 \text{ cm} \times 2.0 \text{ cm}$) was placed inside the quartz cuvette facing visible light (tungsten-halogen light source: 500 W) with 1060 W m^{-2} intensity. Optical absorption spectra were determined upon different light exposure durations using a UV/Vis spectrophotometer (Mikropack DH-2000 with USB4000 detector from Ocean Optics) in order to monitor the rate of degradation by recording the reduction in absorption intensity of methylene blue at the maximum wavelength ($\lambda_{\text{max}} = 615 \text{ nm}$). The degradation efficiency (DE) was calculated as in equation 1:

$$DE = \frac{I_0 - I}{I_0} \times 100 = \frac{C_0 - C}{C_0} \times 100 \quad (1)$$

where I_0 is the initial absorption intensity of methylene blue solution at $\lambda_{\text{max}} = 615 \text{ nm}$ and I is the absorption intensity after photo-degradation. C_0 is the initial concentration of methylene blue solution and C is the concentration after photo-degradation.

2.5.2. Solar photocatalysis test of industrial wastewater

The textile wastewater used in this study was collected from a textile manufacturer, located in Samutprakarn province, Thailand. The textile wastewater had a chemical oxygen demand (COD) = 465 mg L^{-1} , pH = 8.37 and turbidity = 60 NTU.

The experiments of solar photocatalysis of industrial wastewater were conducted in a specially designed wastewater treatment bath as illustrated in Fig. 2 on the top of the building at latitude 14.096 and longitude 100.642. The treatment bath, rectangular in

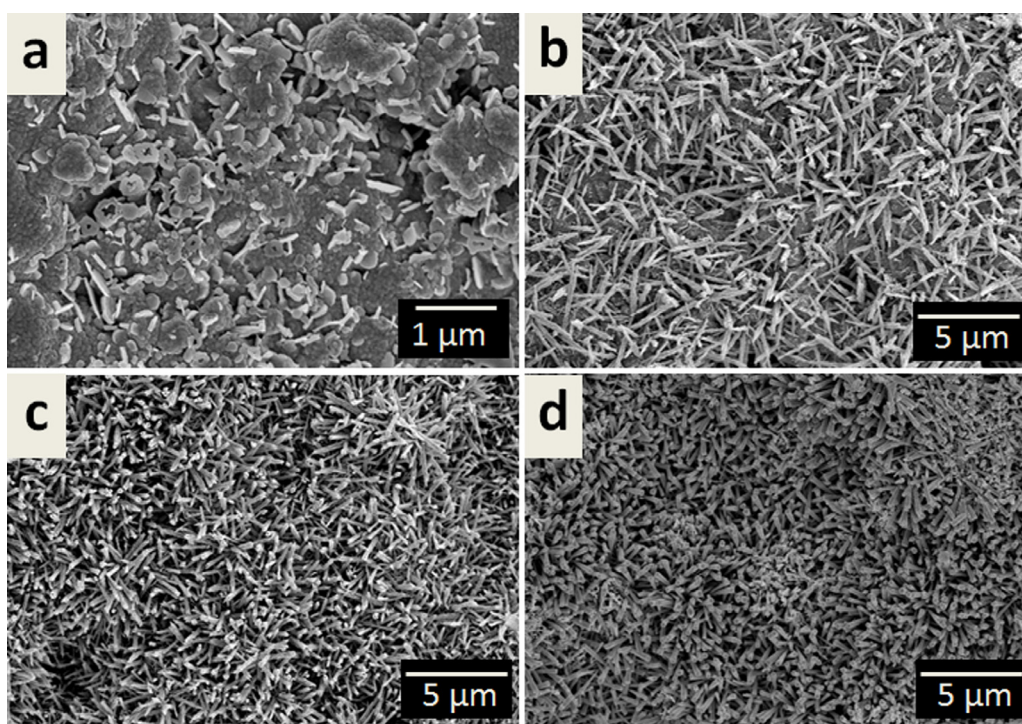


Fig. 3. SEM images of ZnO nanorods grown on porous ceramic substrates through hydrothermal process at 100°C for 15 h with different growth solution concentrations: (a) 1 mM, (b) 5 mM, (c) 10 mM and (d) 20 mM.

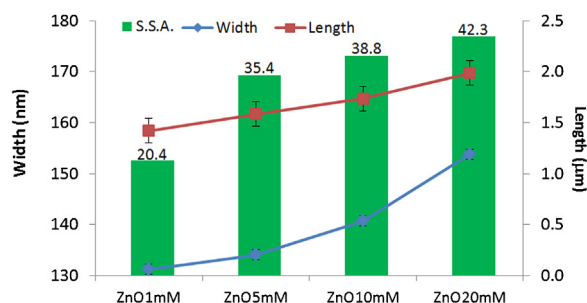


Fig. 4. Width, length and specific surface area of zinc oxide nanorods grown on porous cordierite ceramic supports through hydrothermal process with different growth solution concentrations.

shape, was 20 cm wide, 30 cm long and 5 cm high. The base of treatment bath was 15 degree inclined to the floor in order to allow gravitational flow of wastewater. 8 acrylic plates were placed across the flow direction to enhance the photocatalytic degradation by increasing the contact time of organic molecules in wastewater to the catalysts in the bath. ZnO/ZTO photocatalysts were arranged inside the treatment bath between the acrylic plates. Wastewater flow along the treatment bath was 400 mL/h. Photocatalysis experiments were conducted under sunlight for 3 h per day and the experiment was repeated for 5 days using the natural sunlight during the summer season (April 2013) from 1.00 to 4.00 pm [33]. Absorption spectra of wastewater were determined after different period of exposure to the sunlight using an optical spectrophotometer in order to monitor the rate of degradation as detailed in section 2.5.2.

3. Results and discussion

3.1. Catalyst characterization

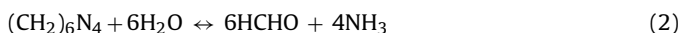
ZnO nanorods grown with different precursor concentrations are shown in Fig. 3. For low precursor concentrations (1 mM of Zn^{2+} solution: ZnO1 mM), ZnO nanorods with low aspect ratio were formed (Fig. 3a) that were 130 nm wide and 1.4 μm long with specific surface area (SSA) of $20.4 \text{ m}^2 \text{ g}^{-1}$ (Fig. 4). At 5 mM and 10 mM precursor concentrations, longer ZnO nanorods of 1.6 μm and 1.7 μm were obtained with higher specific surface areas of 35.4 and $38.8 \text{ m}^2 \text{ g}^{-1}$, respectively (Fig. 3b,c, Fig. 4 and Table 2). At 20 mM precursor solution concentration, dense ZnO nanorods were formed that were 2 μm long, 154 nm wide and showed SSA of $45.3 \text{ m}^2 \text{ g}^{-1}$. From the microstructures of ZnO nanorods, we can conclude that the concentration of growth solution led to approximately two times higher growth in the length of ZnO nanorods compared to the widths. Upon increasing the growth solution concentrations from 1 mM to 20 mM, the nanorod width increased by

Table 2

Specific surface area of as-prepared catalysts and kinetic parameters on the degradation of methylene blue under visible light irradiation upon using as-prepared catalysts.

	SSA ($\text{m}^2 \text{ g}^{-1}$)	Degradation (%)	k (min^{-1})	R^2
ZnO1 mM	35.4	67	0.0083	0.995
ZnO5 mM	35.4	74	0.0082	0.991
ZnO10 mM	38.8	76	0.0093	0.981
ZnO20 mM	45.3	80	0.0146	0.988
ZnO/5ZTO	36.7	93	0.0156	0.989
ZnO/10ZTO	35.5	92	0.0165	0.951
ZnO/15ZTO	34.0	94	0.0165	0.974
ZTO	32.1	79	0.0094	0.984

15%, while 30% longer nanorods were obtained (Fig. 4). This can be related to the decomposition mechanisms of the precursors. One molecule of hexamine gives 4 hydroxyl ions that are twice of the number of Zn^{2+} ions in the equimolar growth solution [34]. Zinc ion requires only two hydroxyl ions to form $\text{Zn}(\text{OH})_2$ that finally transforms to ZnO as shown in equation (2)–(5) [34]. Zn^{2+} and OH^- can also react to form ZnO_2^{2-} and $\text{Zn}(\text{OH})_2$. $\text{Zn}(\text{OH})_2$ reacts with OH^- to form $\text{Zn}(\text{OH})_4^{2-}$. During the hydrothermal growth ZnO_2^{2-} and $\text{Zn}(\text{OH})_2$ form ZnO small particles which aggregate due to large surface energy [35]. The surface energy is substantially reduced when neighboring nanoparticles aggregates or fuses into nanorods which has its own orientation and acts as nuclei for further growth. Zn^{2+} to deposit on the polar surface and. Charged ions in the hydrothermal solution results in attraction toward the polar surface of the ZnO seed layer leading to a preferential growth along the c-axis.



Typical transmission electron microscopy (TEM) images of a ZnO nanorod and nanocomposites of ZnO/10ZTO collected from the monolith ceramic substrate are shown in Figs. 5 and 6. The diffraction pattern taken from a single ZnO nanorod in the inset of Fig. 5a demonstrates a single crystalline wurtzite structure. A high resolution TEM micrograph of a typical ZnO nanorod is also shown in Fig. 5b, with the crystal plane exposed at the surface being visible. Nanocomposite of ZnO nanorods and ZTO are formed by the dissolution of ZnO nanorods and its subsequent re-precipitation in the system wherein Sn^{2+} and OH^- in the solution react with Zn^{2+} supplied from ZnO nanorods forming ZTO (Zn_2SnO_4) as shown in Fig. 6. The lattice fringes of ZTO, as shown in Fig. 6, further show the presence of Zn_2SnO_4 phases in the nano-catalyst, confirming the results obtained from XRD studies.

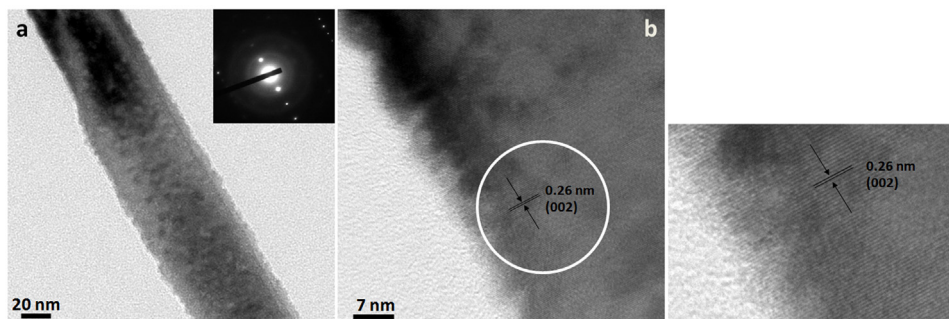


Fig. 5. (a) Transmission electron micrograph of a ZnO nanorod obtained from hydrothermal process at 95 °C using 5 mM growth solution for 15 h. (b) High resolution transmission electron micrograph of a ZnO nanorod showing the crystal plane exposed at the surface.

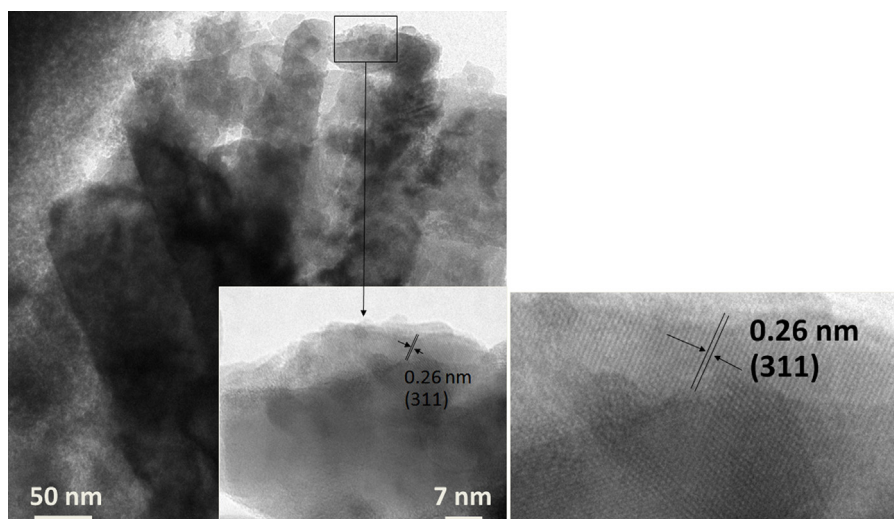


Fig. 6. Transmission electron micrograph of the nanocomposite of ZnO and ZTO (ZnO/10ZTO) obtained from hydrothermal process at 120 °C using 10 mM tin tetrachloride solution at pH 10 for 4 h.

Fig. 7 shows diffractograms of as-annealed ZnO nanorods obtained with different precursor concentrations. The 2θ peaks at 31.77° , 34.42° and 36.26° indicate the existence of zincite structure, which were in good agreement with JCPDF 65-3411. It was also observed that diffraction peak intensities obtained from ZnO nanorods samples increased with an increase of Zn^{2+} concentration in the growth solution, which indicates the formation of more number of ZnO nanorods, agreeing well with the observation made with scanning electron microscopy (Fig. 2 and Fig. 7).

In Fig. 8, we have plotted the XRD of ZnO/ZTO nanocomposites on cordierite substrates. As can be observed, ZTO forms in all samples but a mixed phase with ZnO is obtained. Fig. 9 shows the SEM and EDS results of ZnO/ZTO composite oxides with different fractions of ZnO and ZTO. Fig. 9a is the SEM image of ZnO/5ZTO suggesting the formation of ZTO nanoparticles deposited on the surface of ZnO nanorods. During the synthesis of ZTO, Zn^{2+} ions from the ZnO nanorod surfaces reacted with Sn^{4+} ions available in the precursor solution forming ZTO compounds. When the nanocomposites were synthesized with higher concentration of

tin ion precursor, most of the ZnO nanorod surfaces were transformed to nanocomposite as shown in Fig. 9b and c. This is due to the higher concentration of Sn^{4+} in the growth solution which leads to increased consumption of Zn^{2+} ions released from ZnO nanorods exposing the surfaces to the Sn^{4+} solution to further form ZTO. The X-ray diffractogram of ZnO/ZTO nanocomposite on cordierite substrate (Fig. 9) shows the mixed phases of ZnO and zinc orthostannate (Zn_2SnO_4) that confirmed the transformation of ZnO to Zn_2SnO_4 .

3.2. Photocatalytic activity test

Photocatalytic activities on the degradation of 10 μmol aqueous methylene blue solution using ZnO nanorods and ZnO/ZTO composite oxides grown on ceramic substrates under different synthesis conditions under visible light irradiation for up to 3 h were studied. Fig. 10a shows the photodegradation of methylene blue upon using ZnO nanorods prepared with different precursor concentrations. The inherent surface defects on ZnO crystal lead to the visible light

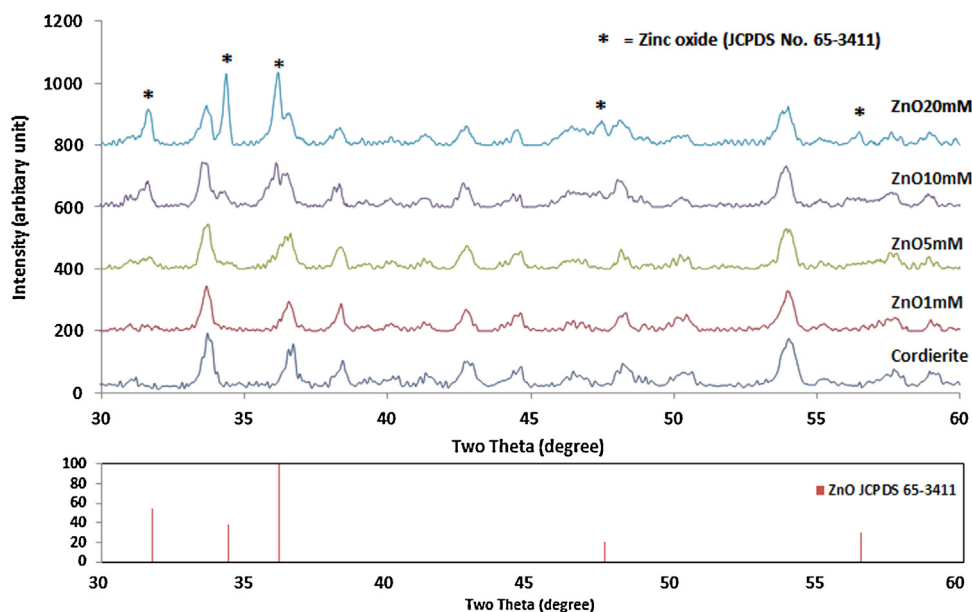


Fig. 7. XRD patterns of ZnO nanorods grown on porous cordierite substrates by hydrothermal process with different growth solution concentrations for 15 h.

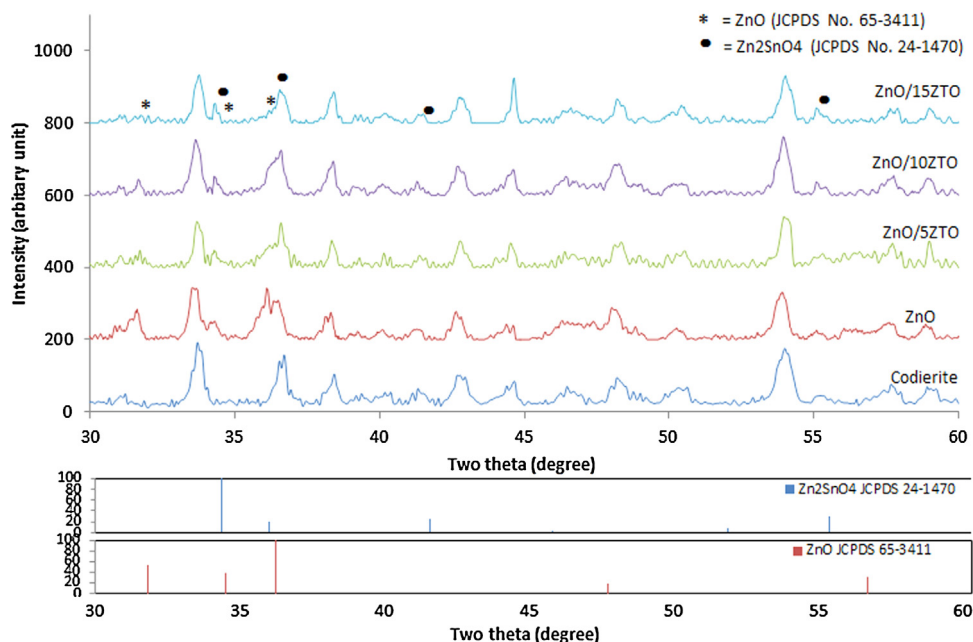


Fig. 8. X-ray diffractogram of ZnO/ZTO nanocomposites on cordierite substrate. The JCPDS data of zinc oxide and zinc orthostannate are plotted in the bottom of the XRD spectra for comparison.

photocatalytic activity [36] that can be further improved by increasing the catalyst surface area. The highest photocatalytic activity was observed upon using the ZnO20 mM catalysts. 80% degradation efficiency of methylene blue was observed upon visible light illumination for 3 h that is 13% more than what was observed using the other ZnO nanorod catalysts. This is attributed to the larger specific surface area of ZnO20 mM ($45 \text{ m}^2 \text{ g}^{-1}$) as given in Table 2. The experiments of self-degradation of methylene blue solution (without photocatalyst) were conducted in order to compare the photodegradation and photocatalytic activity as shown in Fig. 10. It was observed that maximum self-degradation of $10 \mu\text{M}$ methylene blue (MB) under halogen lamp irradiation for 3 h was 38% as shown in Fig. 10.

Coupling ZnO with ZTO enhanced rate of methylene blue degradation as shown in Fig. 10b. It can be seen that more than 60% of

$10 \mu\text{mol}$ methylene blue solutions were degraded within one hour of irradiation under visible light when ZnO/ZTO composites were used and almost 100% degradation was achieved after irradiation for 3 h (Fig. 10b). This can be attributed to the synergistic effect of using multi-oxides enhanced catalytic activity by the reduction of electron–hole recombination due to charge separation [28,29,37]. The energy band diagram of the ZnO/ZTO showing the possible electron–hole pair separation is given in Fig. 11. The presence of higher bandgap ZTO (3.6 eV) nanocrystals bound to ZnO (3.37 eV) nanorods allow the photoexcited electrons to transfer from the conduction band (CB) of ZTO to the CB of ZnO as ZTO is a good electron transport material [38,39], while the holes remain on the ZTO surface, resulting in the reduction of charge recombinations [26]. A further enhancement of 16% in the photocatalytic activity could be achieved by coupling ZnO with ZTO (ZnO/15ZTO). The results

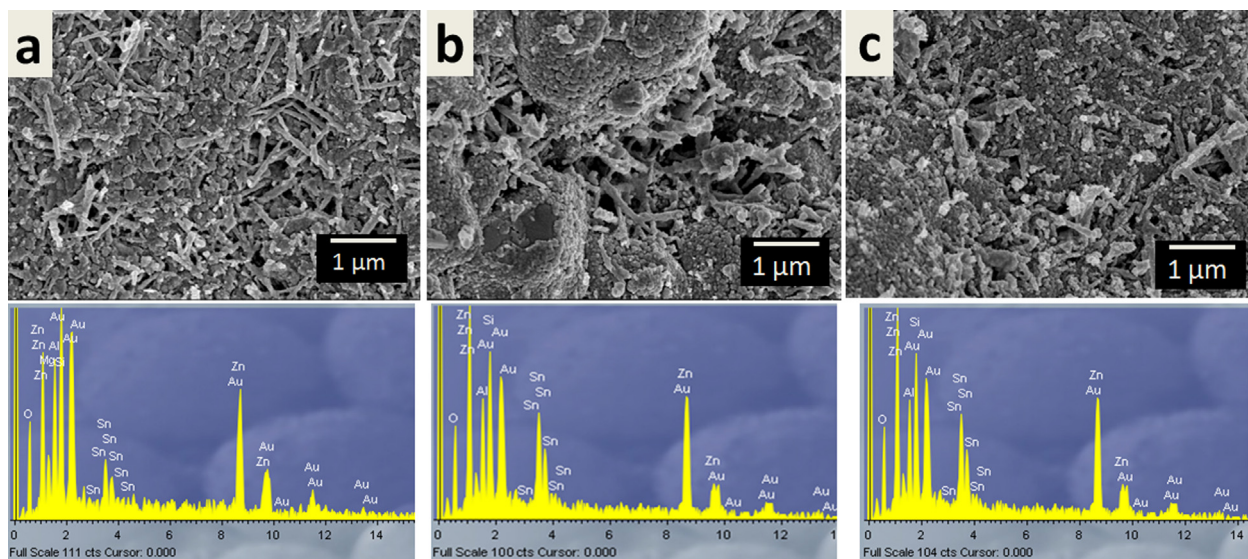


Fig. 9. SEM images and EDS results of ZnO/ZTO composite oxides with different compositions synthesized on ZTO seeded substrate: (a) ZnO/5ZTO, (b) ZnO/10ZTO, (c) ZnO/15ZTO.

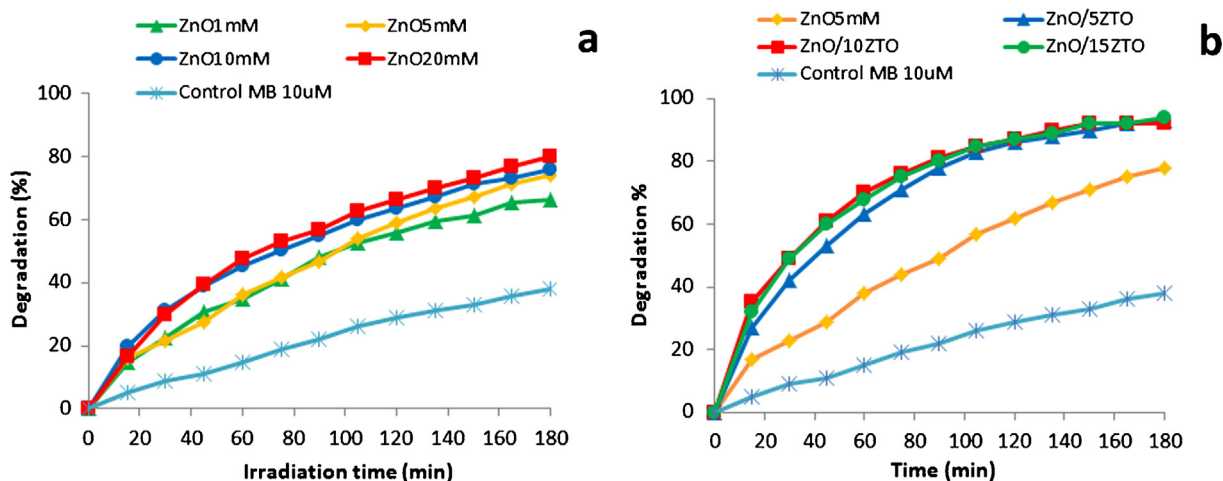


Fig. 10. Photodegradation of methylene blue solution with: (a) ZnO nanorods synthesized from different growth precursor concentrations (control, 1 mM, 5 mM, 10 mM and 20 mM) and (b) ZnO/ZTO composite oxides at different compositions (control, ZnO/5 mMZTO, ZnO/10 mMZTO and ZnO/15 mMZTO).

confirm that ZnO/ZTO nanocomposites are better photocatalysts [8,28]. The absorption peak in the UV region is due to the bandgap transitions and the prolonged absorption tail until ~ 550 nm in the spectrum that results from crystal defects inherently present at the surface of the semiconductor catalyst.

We have also carried out separate experiments for checking the effect of adsorption of methylene blue on the porous substrates, with ZnO and ZnO/ZTO catalysts (ZnO5 mM, ZnO/5ZTO, ZnO/10ZTO and ZnO/15ZTO) by measuring the change of methylene blue concentration after dipping the sample into a 10 μ M methylene blue solution in the dark for a 30 min period. We observe that the nanocomposite catalyst (ZnO/5ZTO) shows the highest methylene blue adsorption ($\sim 6.52\%$), while ZnO, ZnO/10ZTO, ZnO/15ZTO and bare-substrate show slightly lower adsorption (6.43%, 6.47%, 6.21% and 5.18%, respectively), which is related to the effective surface area of the substrates.

Kinetic parameters of visible light degradation of methylene blue with ZnO nanorods and ZnO/ZTO composites are shown in Fig. 10 and summarized in Table 2. The degradation of methylene blue with respect to the irradiation time follows a linear relationship thus showing first order kinetics ($R^2 > 0.95$) (Fig. 12 and Table 2). The slope represents the rate constant of de-colorization (k) that was found to be 0.015 min^{-1} for the ZnO20 mM sample, while upon using ZnO/ZTO composite catalysts, the rate of degradation were found to be $\sim 0.017 \text{ min}^{-1}$. Thus incorporation of ZnO/ZTO interfaces for more efficient charge separation enhances photocatalytic activities. Thus incorporation of ZnO/ZTO interfaces for more efficient charge separation is enhances photocatalytic activities.

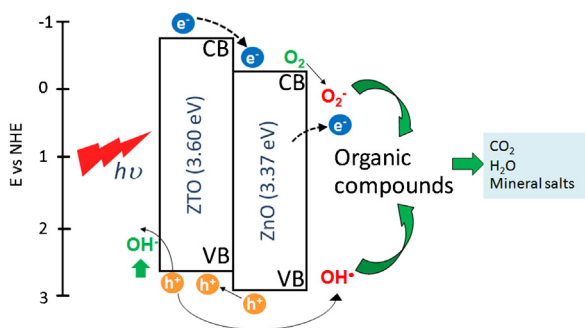


Fig. 11. Possible energy band diagram of ZnO/ZTO nanocomposite showing the photoexcited electron transfer from higher energy level CB of ZTO to lower energy level CB of ZnO.

3.3. Textile wastewater treatment

ZnO/15ZTO photocatalyst was used to study the degradation of textile wastewater under sunlight. The procedure for photocatalytic degradation measurement of wastewater was similar to the degradation of methylene blue as described in section 2.5.1; only the measured wavelength was changed to 400 nm. The experiments were conducted for 5 days with the same set of photocatalysts but wastewater was replenished every day. The degradation efficiencies were found to be about 50% and stable over 5 days (Fig. 13a). Temperatures of wastewater during the experiments were recorded and plotted as shown in Fig. 13b. Initial temperature was about 28°C which was found to gradually increase to about 50°C upon solar irradiation for 90 min. Identical experiments were conducted to study the solar degradation of 10 μmol of methylene blue for 3 h. We found that solar degradation efficiency of wastewater (50% solar degradation) was lower than the degradation of methylene blue ($\sim 87\%$ degradation) that can be due to the mixtures of dyes in textile wastewater. Different functional groups of dyes influence the degradation mechanisms [40] leading to a complicated degradation process. Table 3 shows the properties of textile wastewater before and after solar photocatalytic treatment using ZnO/15ZTO catalyst. It can be observed that more than 75% COD and 90% turbidity of wastewater can be reduced after only 3 h of exposure to the sun light in the presence

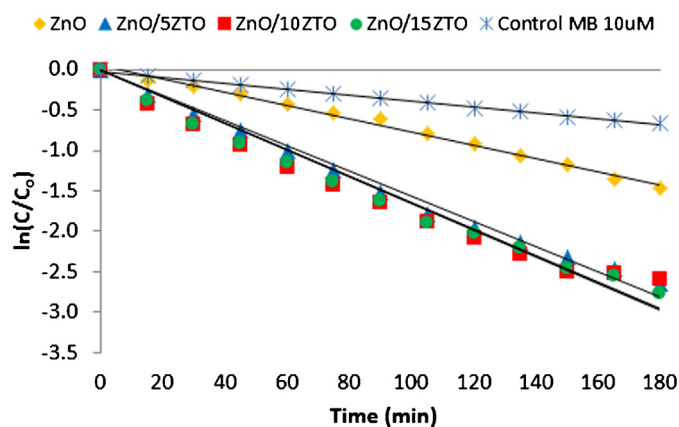


Fig. 12. Kinetic parameters of the degradation of methylene blue with and without using ZnO/ZTO composite oxides at different compositions (control, ZnO/5ZTO, ZnO/10ZTO and ZnO/15ZTO).

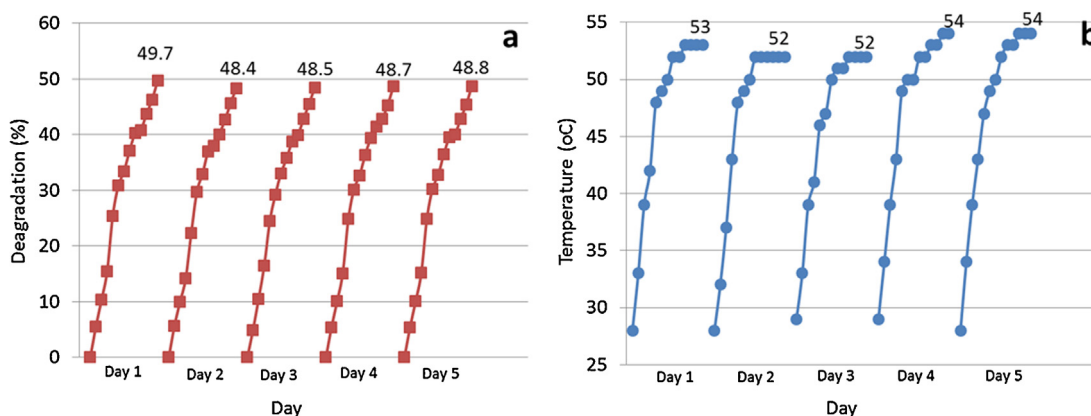


Fig. 13. Solar photocatalytic degradation of textile wastewater collected from discharge of textile industry in Thailand; (a) photodegradation and (b) wastewater temperature during the experiment.

Table 3

Properties of textile wastewater before and after treatment by solar photocatalytic degradation.

	As-received wastewater	After 3 h solar irradiation
COD (mg L ⁻¹)	465	105
pH	8.37	8.24
Conductivity (mS)	6.86	6.53
Turbidity (NTU)	60	<5

of the photocatalysts. Thus, ZnO/ZTO can be ideal supported photocatalysts for solar photocatalytic application using sunlight.

In summary, the synthesis of ZnO nanorods and ZnO/ZTO composite oxides on porous ceramic substrates by a hydrothermal process was studied. The as-prepared catalysts can be attractive candidates for solar photocatalysis. Comparative results of photocatalytic degradation tests on methylene blue under visible light irradiation presented that larger specific surface area ZnO nanorods catalyst (ZnO20 mM) is 13% more active than ZnO nanorods synthesized with 5 mM reactants. A further 16% enhancement in the photocatalytic activity could be achieved by coupling the ZnO nanorods with ZTO that was attributed to the enhanced charge separation. Moreover, ZnO/15ZTO catalyst was applied to treat textile wastewater and almost 50% degradation efficiency and 75% COD removal could be achieved within 3 h of irradiation of sunlight. The photocatalysts were active for repeated treatment of wastewater and no visible reduction in degradation efficiency was observed after using the photocatalysts for 5 days.

Acknowledgments

The authors would like to acknowledge partial financial support from the National Research Council of Thailand (NRCT), National Metal and Materials Technology Center (MTEC) belonging to the National Science & Technology Development Agency (NSTDA), Thailand. JD would like to thank the Research Council of Oman for partial financial support under the Chair in Nanotechnology Programme of TRC.

References

[1] J. Easton, *The Dye Maker's View*, Society of Dyes and Colourists, Bradford, UK, 1995.
[2] Y.M. Slokar, A. Majcen Le Marechal, *Dyes Pigments* 37 (1998) 335–356.

[3] W.-J. Lau, A.F. Ismail, *Desalination* 245 (2009) 321–348.
[4] W.B. Group, *Environmental, Health, and Safety Guidelines-Textile Manufacturing*, 2007.
[5] S.W. Powell, *Method for Electrocoagulation of Liquids*, United State, 2002.
[6] J. Strunk, K. Kaher, X. Xia, M. Muhler, *Surf. Sci.* 603 (2009) 1776–1783.
[7] F.W. Gilmore, *Electrocoagulation Chamber and Method*, United States, 2003.
[8] R. Ullah, J. Dutta, *J. Hazard. Mater.* 156 (2008) 194–200.
[9] J. Huang, X. Xu, C. Gu, W. Wang, B. Geng, Y. Sun, J. Liu, *Sensors Actuators B: Chem.* 173 (2012) 599–606.
[10] A.M. Ali, E.A.C. Emanuelsson, D.A. Patterson, *Appl. Catal. B: Environ.* 97 (2010) 168–181.
[11] S.K. Pardeshi, A.B. Patil, *J. Mol. Catal. A: Chem.* 308 (2009) 32–40.
[12] M. Mahmood, J. Dutta, *J. Sol-Gel Sci. Technol.* 62 (2012) 495–504.
[13] Gary A. Tipton, H.M. Slack, *Cells and Electrodes for Electrocoagulation Treatment of Waste Water*, United State, 2005.
[14] S. Baruah, J. Dutta, *Sci. Technol. Adv. Mater.* 10 (2009) 013001.
[15] G.L. Hornyak, J.T.H.F. Dutta, *Introduction to Nanoscience*, CRC Press, 2008.
[16] B. Cheng, E.T. Samulski, *Chem. Commun.* (2004) 986–987.
[17] S. Baruah, J. Dutta, *J. Cryst. Growth* 311 (2009) 2549–2554.
[18] L.E. Greene, M. Law, D.H. Tan, M. Montano, J. Goldberger, G. Somorjai, P. Yang, *Nano Lett.* 5 (2005) 1231–1236.
[19] Paul E. Morkovsky, S. Douglas D. Kaspar, J.M. Petru, *Process and Apparatus for Electrocoagulative Treatment of Industrial Waste Water*, Kaspar Electroplating Coporation, United State, 1999.
[20] J. Song, S. Lim, *J. Phys. Chem. C* 111 (2006) 596–600.
[21] M. Vaseem, K.M. Lee, D.Y. Kim, Y.-B. Hahn, *Mater. Chem. Phys.* 125 (2011) 334–341.
[22] Z. Jing, J. Wang, F. Li, L. Tan, Y. Fu, Q. Li, *J. Nanoeng. Nanomanufact.* 2 (2012) 133–142.
[23] X. Fu, X. Wang, J. Long, Z. Ding, T. Yan, G. Zhang, Z. Zhang, H. Lin, X. Fu, *J. Solid State Chem.* 182 (2009) 517–524.
[24] L. Guo, Y.L. Ji, H. Xu, P. Simon, Z. Wu, *J. Am. Chem. Soc.* 124 (2002) 14864–14865.
[25] A.T. Al-Hinai, M.H. Al-Hinai, J. Dutta, *Mater. Res. Bull.* 49 (2014) 645–650.
[26] W.W. Wang, Y.J. Zhu, L.X. Yang, *Adv. Funct. Mater.* 17 (2007) 59–64.
[27] S. Danwittayakul, M. Jaisai, T. Koottatep, J. Dutta, *Ind. Eng. Chem. Res.* 52 (2013) 13629–13636.
[28] N. Modirshahla, A. Hassani, M.A. Behnajady, R. Rahbarfam, *Desalination* 271 (2011) 187–192.
[29] G. Yang, Z. Yan, T. Xiao, *Appl. Surf. Sci.* 258 (2012) 8704–8712.
[30] S. Danwittayakul, J. Dutta, *Int. J. Hydrogen Energy* 37 (2012) 5518–5526.
[31] A. Sugunan, H.C. Warad, M. Boman, J. Dutta, *J. Sol-Gel Sci. Technol.* 39 (2006) 49–56.
[32] S. Danwittayakul, J. Dutta, *J. Alloys Compd.* 586 (2014) 169–175.
[33] C. Sirisamphanwong, N. Ketjoy, W. Rakwichain, S. Vaivudh, *Int. J. Renewable Energy* 6 (2011) 25–29.
[34] S. Baruah, M.A. Mahmood, M.T. Myint, T. Bora, J. Dutta, *Beilstein J. Nanotechnol.* 1 (2010) 14–20.
[35] J. Lian, Z. Ding, F.-I. Kwong, D.H.L. Ng, *CrystEngComm* 13 (2011) 4820–4822.
[36] S. Baruah, S.S. Sinha, B. Ghosh, S.K. Pal, A.K. Raychaudhuri, J. Dutta, *J. Appl. Phys.* 105 (2009) 074308–074314.
[37] M.A. Alpuche-Aviles, Y. Wu, *J. Am. Chem. Soc.* 131 (2009) 3216–3224.
[38] K. Nomura, H. Ohta, K. Ueda, T. Kamiya, M. Hirano, H. Hosono, *Microelectron. Eng.* 72 (2004) 294–298.
[39] S. Rehman, R. Ullah, A.M. Butt, N.D. Gohar, *J. Hazard. Mater.* 170 (2009) 560–569.
[40] S. Chakrabarti, B.K. Dutta, *J. Hazard. Mater.* 112 (2004) 269–278.